Influence of Dy Doping on Electrical Properties and dc Aging Behaviors of Zn-Pr-Co-Cr System

Choon-Woo Nahm[a]
Department of Electrical Engineering, Dongeui University, Gaya 3-dong, Busanjin-gu, Busan 614-714, Korea

[a]E-mail : cwnahm@deu.ac.kr

(Received August 24 2007, Accepted December 17 2007)

The electrical properties and dc aging behavior for specified stress state of system, which is composed of quaternary Zn-Pr-Co-Cr, were investigated for different Dy_2O_3 addition doping level. As Dy_2O_3 doping level increased, the density decreased in the range of 5.51-4.90 g/cm^3, reaching maximum at 0.5 mol% and the average ZnO grain size decreased in the range of 17.7-6.0 μm. The incorporation of Dy_2O_3 significantly improved the non-ohmic properties, above 30 in non-ohmic coefficient, compared with that of undoped samples. The samples with the best performance of non-ohmic properties were obtained for Dy_2O_3 doping level of 1.0 mol%, with 49 in non-ohmic coefficient and 2.6 μA/cm^2 in leakage current. The samples with the highest stability were obtained for Dy_2O_3 doping level of 0.5 mol%.

Keywords : Microstructure, Electrical properties, Varistors, Pr_6O_{11}; Dy_2O_3

1. INTRODUCTION

Many electronic devices and electric power systems can be subjected to voltage transients (called surges) induced by lightning, switching, and electrostatic discharge. They are vulnerable to damage by surges in excess of their voltage ratings, because of weakness of insulating strength. This is severe problem. One way to overcoming this is to use the varistors. ZnO varistors are ceramic semiconductor components made by ZnO powder containing minor additives. This is one of well-known MOVs (Metal-Oxide-Varistors). They exhibit highly non-ohmic voltage-current (V-I) characteristics expressed by $J = K \cdot E^{\alpha}$, where K is a constant and α is non-ohmic coefficient as an index or figure of merit indicating the effectiveness of a varistor. Furthermore, they possess excellent high energy-handling capabilities. As a result, they have been widely applied as to protect different semiconductor devices, electronic circuits, and electric power systems from dangerous abnormal transient voltage[1,2]. The non-ohmic properties of ZnO varistors are attributed to a double Schottky barrier (DSB) formed at active grain boundaries containing many trap states.

ZnO varistors containing Pr_6O_{11} as VFO have been actively studied[3-12]. Nahm et al. reported that ZnO-Pr_6O_{11}-CoO-Cr_2O_3-M_2O_3 (M = Er, Y, Dy, La)-based varistors have highly non-ohmic properties[5,7,9,10]. To develop the varistors of high performance, it is very important to comprehend the effects of the dopant, doping level, and process on non-ohmic properties.

The purpose of this work is to investigate the effect of Dy doping on electrical properties and dc accelerated aging behaviors of the quaternary Zn-Pr-Co-Cr system.

2. EXPERIMENTAL PROCEDURE

2.1 Sample preparation

Reagent-grade raw materials were prepared for system with composition (96.0-x) mol% ZnO, 0.5 mol% Pr_6O_{11}, 3.0 mol% CoO, 0.5 mol% Cr_2O_3, x mol% Dy_2O_3 (x = 0.0-2.0). Raw materials were mixed by ball milling with zirconia balls and acetone in a polypropylene bottle for 24 h. The mixture was dried at 120 °C for 12 h and calcined in air at 750 °C for 2 h. The calcined mixture was pulverized using an agate mortar/pestle and after 2 wt% polyvinyl alcohol (PVA) binder addition, granulated by sieving 200-mesh screen to produce starting powder. The powder was uniaxially pressed into discs of 10 mm in diameter and 2 mm in thickness at a pressure of 800 kg/cm^2. The discs were covered with raw powder in alumina crucible, sintered at 1350 °C for 1 h. The heating rate and cooling rate were 4 °C/min. The sintered samples were lapped and polished to 1.0 mm thickness. The final samples were about 8 mm in diameter and 1.0 mm in thickness. Silver paste was coated on both faces of samples and ohmic contact of electrodes was formed by heating at 600 °C for 10 min. The electrodes were 5 mm in diameter.

2.2 Microstructure examination

The either surface of samples was lapped and ground with SiC paper and polished with 0.3 μm-Al_2O_3 powder to a mirror-like surface. The polished samples were thermally etched at 1100 °C for 30 min. The surface microstructure was examined by a scanning electron microscope (SEM, Hitachi S2400, Japan). The average grain size (d) was determined by the lineal intercept method, given by d = 1.56L /MN, where L is the random line length on the micrograph, M is the magnification of the micrograph, and N is the number of the grain boundaries intercepted by lines[13]. The crystalline phases were identified by an X-ray diffractometry (XRD, Rigaku D/max 2100, Japan) with CuK_α radiation. The density (ρ) of ceramics was measured by the Archimedes method.

2.3 E-J characteristic measurement

The E-J characteristics of the system were measured using a high voltage source measure unit (Keithley 237). The electric field ($E_{1\ mA}$) was measured at a current density of 1.0 mA/cm^2 and the leakage current (J_L) was measured at 0.80 $E_{1\ mA}$. In addition, the non-ohmic coefficient (α) is defined by the empirical law, $J = K \cdot E^\alpha$, where J is the current density, E is the applied electric field, and K is a constant. α was determined in the current density range of 1.0 mA/cm^2 to 10 mA/cm^2, where $\alpha = 1/(\log E_2 - \log E_1)$, and E_1 and E_2 are the electric field corresponding to 1.0 mA/cm^2 and 10 mA/cm^2, respectively.

2.4 DC accelerated aging measurement

The stability against DC accelerated aging stress was performed under the four continuous states;

(i) 1st stress: 0.85 $V_{1\ mA}$/115 °C/24 h,

(ii) 2nd stress: 0.90 $V_{1\ mA}$/120 °C /24 h,

(iii) 3rd stress: 0.95 $V_{1\ mA}$/125 °C /24 h,

(iv) 4th stress: 0.95 $V_{1\ mA}$/150 °C /24 h.

Simultaneously, the leakage current during the stress time was monitored at intervals of 1 min by a high voltage source-measure unit (Keithley 237). The system stressed was applied to the electrical characteristics after storage at normal room temperature for 2 h. The degradation rate coefficient (K_T) was calculated from the following equation[14], $I_L = I_{Lo} + K_T t^{1/2}$, where I_L is the leakage current at stress time (t) and I_{Lo} is I_L at t = 0. After the respective stresses, the V-I characteristics were measured at room temperature. In treatment of numerical data, 5 samples for system (sintered at the same time) were used for all electrical measurements and their average value is presented.

3. RESULTS AND DISCUSSION

3.1 Microstructure

Figure 1 shows SEM micrographs of system for different Dy_2O_3 doping level. When Dy_2O_3 doping level increased in less than 0.5 mol%, the sintered density increased in the range of 5.38-5.51 g/cm^3 corresponding to 93-95 % of theoretical density (TD = 5.78 g/cm^3 in

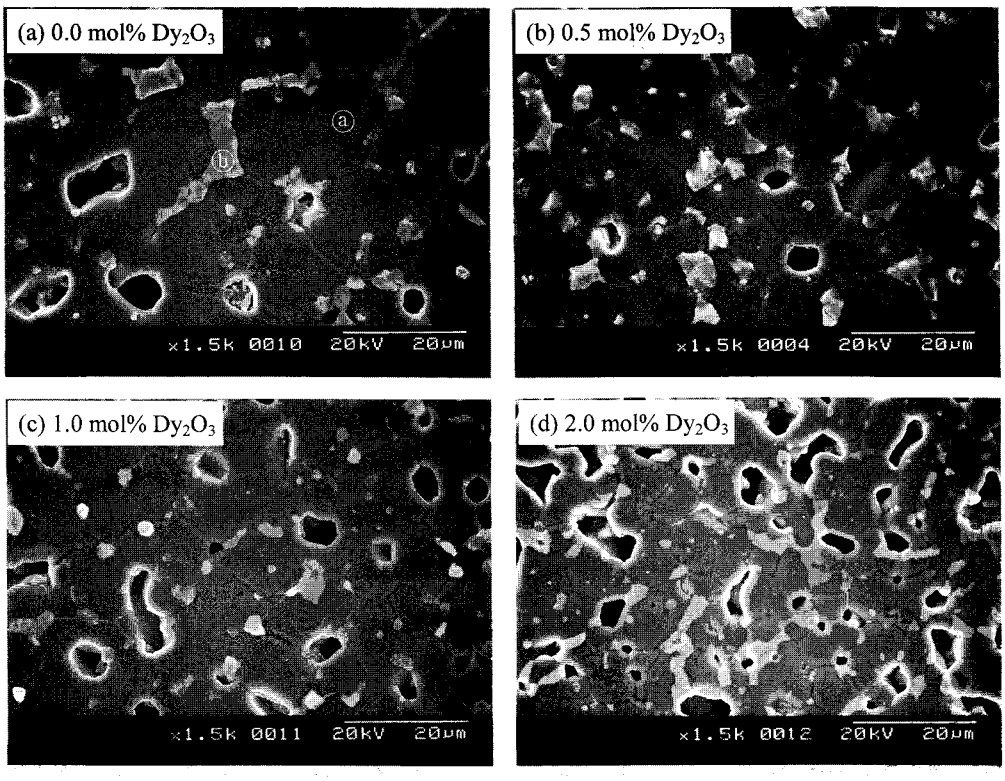

Fig. 1. SEM micrographs for different Dy_2O_3 doping level; ⓐ ZnO grain and ⓑ intergranular layer.

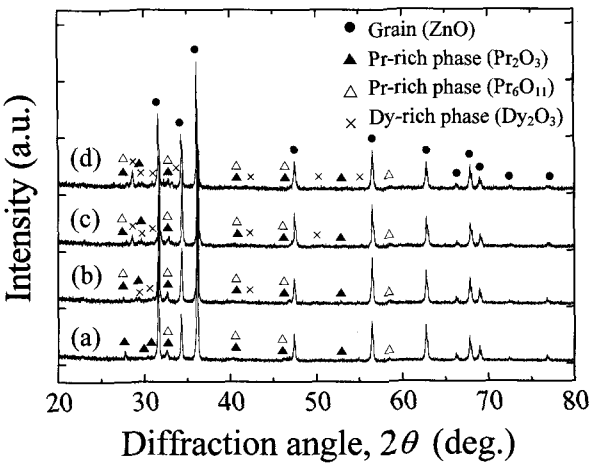

Fig. 2. XRD patterns for different Dy_2O_3 doping level; (a) 0.0 mol%, (b) 0.5 mol%, (c) 1.0 mol%, and (d) 2.0 mol%.

ZnO). However, when Dy_2O_3 doping level increased in more than 0.5 mol%, the sintered density decreased in the range of 5.40-4.90 g/cm^3. It is assumed that the increase of sintered density with increasing Dy_2O_3 doping level less than 0.5 mol% is related to the formation of liquid-phases. Liquid-phase sintering in ZnO-Pr_6O_{11}-CoO system is affected by Pr/Co composition. A. B. Alles, etc reported that liquid-phase is formed at 1350 °C when Pr/Co is in the range of 1/1-1/4[15]. Therefore, Pr/Co=1/6 composition in this paper will sufficiently cause liquid-phase at 1350 °C. However it is assumed that Dy_2O_3 doping will affect liquid-phase formation, which Dy_2O_3 concentration more than 0.5 mol% may prevent liquid-phase even at 1350 °C. As a result, the samples doped with 0.5 mol% in Dy_2O_3 doping level exhibited the highest sintered density. The average grain size was linearly decreased from 17.7 to 6.0 μm with the increase of Dy_2O_3 doping level, as indicated in Fig. 4. It is supposed that this is attributed to the secondary phases generated by segregating at grain boundaries and nodal points with the increase of Dy_2O_3 doping level. It is confirmed from XRD shown in Fig. 2 that secondary phases are the mixture of Pr- and Dy-rich phases. All systems was consisted of only two phases, i.e. ZnO grain and intergranular layer as a secondary phase comprising of Pr oxide and Dy_2O_3 regardless of Dy_2O_3 doping level.

3.2 E-J characteristics

Figure 3 shows the electric field-current density (E-J) characteristics of samples for different Dy_2O_3 doping level. The non-ohmic properties are characterized by non-ohmicity in the E-J characteristics. The curves show the conduction characteristics divide into two regions: an ohmic region before breakdown and a non-ohmic region after breakdown. The sharper the knee of the curves between the two regions, the better the non-ohmic

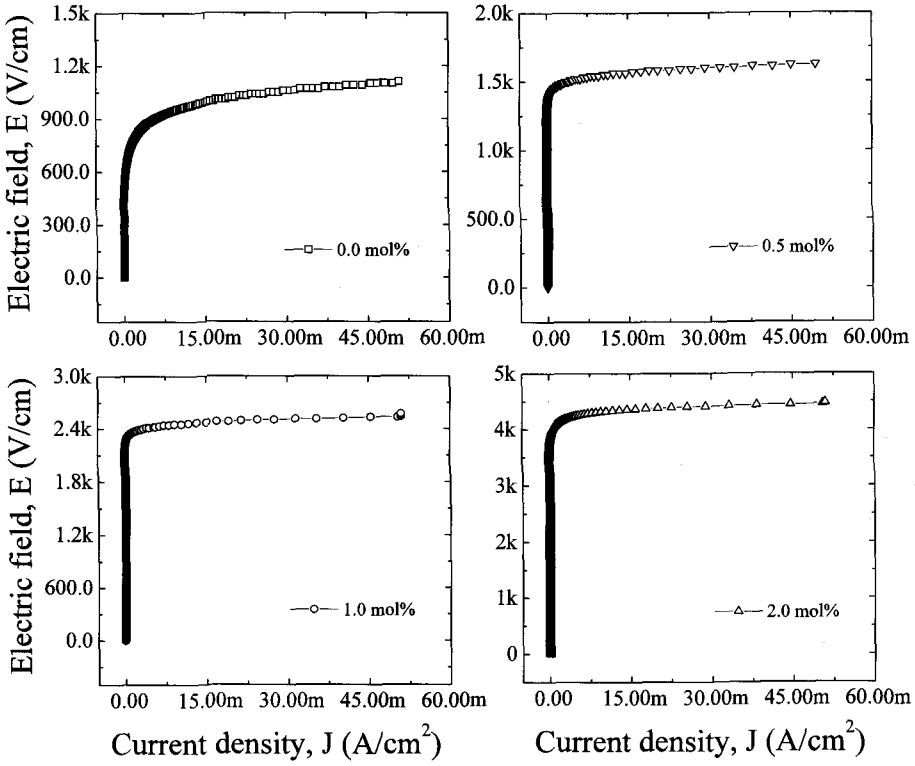

Fig. 3. E-J characteristics for different Dy_2O_3 doping level.

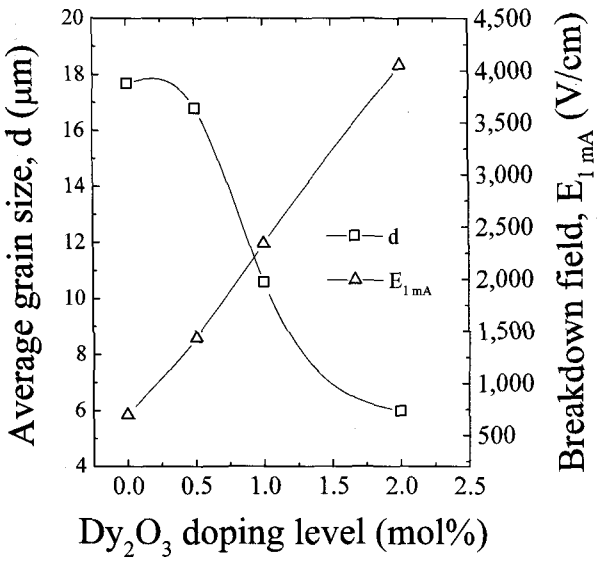

Fig. 4. Average grain size and Breakdown field as a function of Dy_2O_3 concentration.

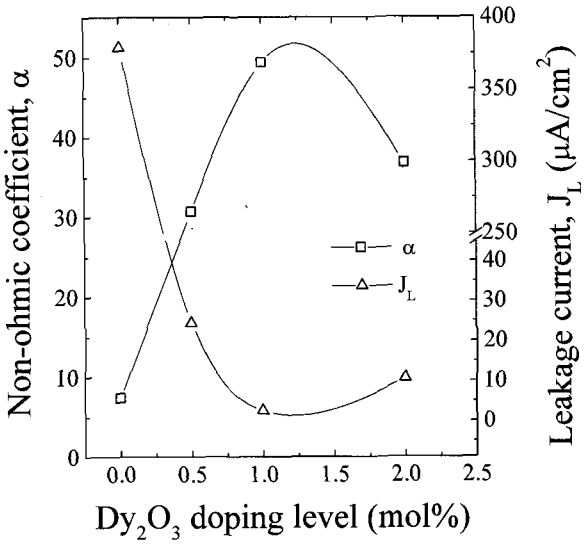

Fig. 5. Non-ohmic coefficient and leakage current as a function of Dy_2O_3 concentration.

properties. It can be seen that the knee region of E-J curves of the doped samples is much keener than that of the undoped samples. The undoped samples showed poor non-ohmic properties. On adding more Dy_2O_3, the knee gradually becomes more pronounced and the non-ohmic properties are enhanced. Therefore, the incorporation of Dy_2O_3 seems to remarkably enhance non-ohmic properties.

Figure 4 shows the breakdown field ($E_{1\,mA}$) and the average grain size (d) of the samples as a function of Dy_2O_3 concentration. The $E_{1\,mA}$ was greatly increased in the range of 699-4053 V/cm with the increase of Dy_2O_3 doping level. The increase of $E_{1\,mA}$ with increasing Dy_2O_3 concentration can be explained by the increase in the number of grain boundaries owing to the reduction in the average ZnO grain size. The breakdown voltage per grain boundaries (V_{gb}) of the doped samples was in the range of 2-3 V/gb, whereas the undoped samples were only 1.2 V/gb. Therefore, it is assumed that the undoped samples have poor grain boundaries. These grain boundaries cause very low non-ohmic properties.

Figure 5 shows the non-ohmic coefficient (α) and the leakage current (J_L) of the samples as a function of Dy_2O_3 concentration. The α and J_L values are derived from the E-J curves shown in Fig. 3. The α value of undoped samples was only 7.4, whereas the α value of the doped samples significantly increased to above 30. The α value increased up to 1.0 mol% in Dy_2O_3 concentration, whereas further doping decreased it. The maximum non-ohmic coefficient was 49.4, which was obtained for 1.0 mol% in Dy_2O_3 doping level. It is assumed that the increase of α increasing Dy_2O_3 concentration is attributed to predominant tunneling current due to the increase of barrier height at the grain boundaries. The J_L value of the undoped samples was 379.1 μA/cm^2, whereas the J_L value of the doped samples very abruptly decreased in the range of 2.6-24.5 μA/cm^2. The minimum value of J_L was 2.6 μA/cm^2 which obtained for 1.0 mol% in Dy_2O_3 doping level. It can be seen that the variation of J_L shows the inverse relationship to the variation of α. This is because the high α value leads to low leakage current due to relatively high tunneling current and the low α value leads to high leakage current due to relatively high thermionic emission current. As a result, the incorporation of Dy_2O_3 was confirmed to significantly improve the non-ohmic properties.

3.3 DC accelerated aging characteristics

Figure 6 shows leakage current during DC accelerated aging stress for different Dy_2O_3 doping level. Each sample shows different behavior for DC accelerated aging stress. This means Dy_2O_3 doping level affects resistance against stress. The samples doped with 2.0 mol% in Dy_2O_3 concentration exhibited the thermal runaway within a short time for the first stress (0.85 $E_{1\,mA}$/115 °C/24 h). The samples stressed were completely degraded. This poor stability may be attributed to the low density, which decreases the number of current conduction path, and it eventually leads to the concentration of current. The samples doped with 1.0 mol% in Dy_2O_3 concentration exhibited a high stability until the second stress (0.90 $E_{1\,mA}$/120 °C/24 h), and highly positive creep of leakage current during the third stress (0.95 $E_{1\,mA}$/125 °C/24 h). These samples finally exhibited the thermal runaway during the fourth stress

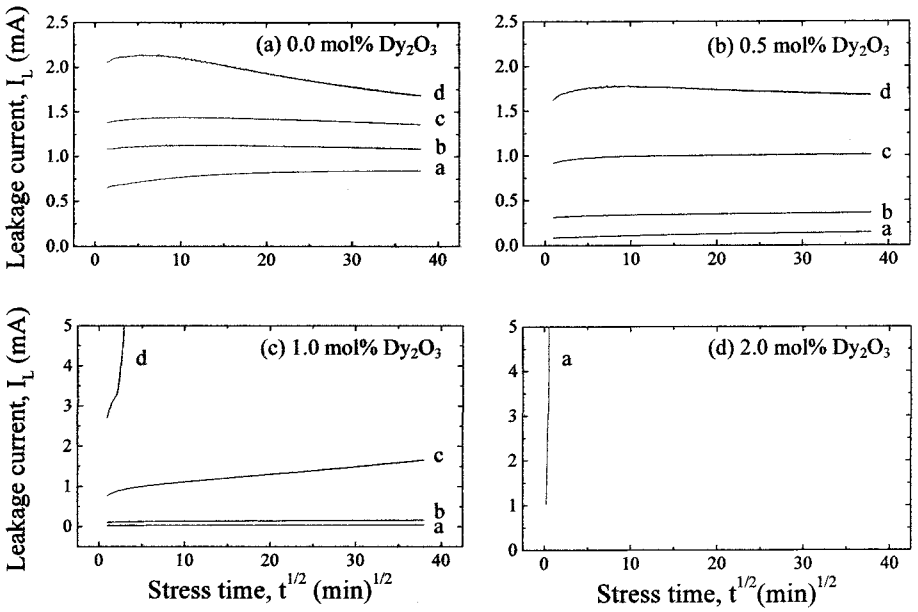

Fig. 6. Leakage current during DC accelerated aging stress for different Dy_2O_3 doping level.

(0.95 $E_{1\,mA}$/150 °C/24 h). This is also due to the sintered density which is not so high, although it is low leakage current, as mentioned just previously. The undoped samples exhibited weak positive creep phenomena of the leakage current during the first stress (0.85 $E_{1\,mA}$/115 °C/24 h). Thereafter, they showed negative creep phenomena. Although these samples have very high leakage current, to not cause the thermal runaway is like to due to ohmic-like properties, which is low non-ohmicity. On the other hand, the samples doped with 0.5 mol% in Dy_2O_3 concentration exhibited much better stability, compared with the samples for different Dy_2O_3 doping level. They exhibited very weak positive creep of leakage current until the third stress (0.95 $E_{1\,mA}$/125 °C/24 h), but they exhibited rather weak negative creep of leakage current during the fourth stress (0.95 $E_{1\,mA}$/150 °C/24 h).

The stability of samples can be estimated by the degradation rate coefficient (K_T), indicating the degree of aging. The lower the K_T, the higher the stability. For samples doped with 0.5 mol% in Dy_2O_3 concentration, the K_T was 8.6 $\mu A \cdot h^{-1/2}$ after the first stress (0.85 $E_{1\,mA}$/115 °C/24 h), 5.9 $\mu A \cdot h^{-1/2}$ after the second stress (0.90 $E_{1\,mA}$/120 °C/24 h), 4.9 $\mu A \cdot h^{-1/2}$ after the third stress (0.95 $E_{1\,mA}$/125 °C/24 h). Furthermore, the K_T was -27.5 $\mu A \cdot h^{-1/2}$ after the fourth stress (0.95 $E_{1\,mA}$/150 °C/24 h). As a result, the K_T value decreased in accordance with increasing strength for stress. The detailed K_T variation for different Dy_2O_3 doping level is shown in Fig. 7. The reason why the samples doped with 0.5 mol% in Dy_2O_3 concentration exhibit high stability may be macroscopically attributed to high sintered density,

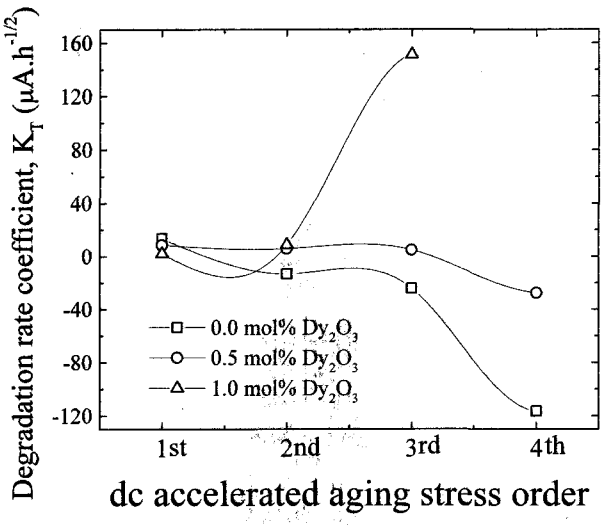

Fig. 7. Degradation rate coefficient for different Dy_2O_3 doping level.

even though it is relatively high leakage current, compared with other samples, and microscopically to the restriction of zinc interstitial (Zn_i) migration within depletion layer or the stabilization of interface states by properly doping Dy_2O_3.

The E-J characteristic parameters, the variation of electric field, variation (%$\triangle E_{1\,mA}$) of non-ohmic coefficient (%$\triangle\alpha$), and variation of leakage current density (%$\triangle J_L$) after dc accelerated aging stress are summarized in Table 1. The samples doped with 0.5 mol% in Dy_2O_3 concentration exhibit high stability, with

Table 1. E-J characteristic parameters before and after dc accelerated aging stress for different doping level.

Dy_2O_3 concentration (mol%)	Stress state	K_T ($\mu A \cdot h^{-1/2}$)	$E_{1\,mA}$ (V/cm)	$\%\triangle E_{1\,mA}$	α	$\%\triangle\alpha$	J_L ($\mu A/cm^2$)	$\%\triangle J_L$
0.0	before		699	0	7.4	0	379.1	0
	1st	13.5	570	-18.5	5.6	-24.3	449	18.4
	2nd	-13.1	570	-18.5	5.6	-24.3	445.9	17.6
	3rd	-24.1	576	-17.6	5.8	-21.6	441.3	16.4
	4th	-116.4	626	-9.0	6.4	-13.5	413.8	9.2
0.5	before		1434	0	30.7	0	24.5	0
	1st	8.6	1384	-3.5	27.0	-12.1	44.4	81.2
	2nd	5.9	1371	-4.4	25.9	-15.6	52.6	114.7
	3rd	4.9	1357	-5.4	24.6	-19.9	67.9	177.1
	4th	-27.5	1406	-2.0	24.8	-19.2	73.5	195.9
1.0	before		2340	0	49.4	0	2.6	0
	1st	2.1	2295	-1.9	45.0	-8.9	5.6	115.4
	2nd	8.8	2270	-3.0	40.9	-17.2	7.1	173.1
	3rd	151.3	2215	-5.3	34.5	-30.2	9.2	253.8
	4th	Thermal runaway						
2.0	before		4053	0	36.8	0	10.7	0
	1st	Thermal runaway						

+2.0 % in $\%\triangle E_{1\,mA}$, -19.2 % in $\%\triangle\alpha$, and +195.9 % in $\%\triangle J_L$ for stress state of 0.95 $E_{1\,mA}$/150 °C/24 h.

4. CONCLUSION

The electrical characteristics and dc accelerated aging behaviors of Zn-Pr-Co-Cr system were investigated for different Dy_2O_3 doping level. The sintered density increased up to 0.5 mol% in Dy_2O_3 concentration and further doping decreased the sintered density. The non-ohmic coefficient increased up to 1.0 mol% in Dy_2O_3 concentration and further doping decreased the non-ohmic coefficient. The maximum non-ohmic coefficient was 49.4 for 1.0 mol% in Dy_2O_3 concentration. The dc accelerated aging characteristics of the doped samples were worse with the increase of Dy_2O_3 doping level. The highest resistance against stress was obtained for 0.5 mol% in doping level, with in $\%\triangle E_{1\,mA}$ = +2.0 %, $\%\triangle\alpha$ = -19.2 % , and $\%\triangle J_L$ = +195.9 % for stress state of 0.95 $E_{1\,mA}$/150 °C/24 h. In conclusion, the stability against DC accelerated aging stress seems to be affected more predominantly by sintered density than leakage current.

REFERENCE

[1] L. M. Levinson and H. R. Philipp, "Zinc oxide varistor-a review", Amer. Ceram. Soc. Bull., Vol. 65, No. 4, p. 639, 1986.

[2] T. K. Gupta, "Application of zinc oxide varistor", J. Amer. Ceram. Soc., Vol. 73, No. 7, p. 1817, 1990.

[3] A. B. Alles and V. L. Burdick, "The effect of liquid-phase sintering on the properties of Pr_6O_{11}-based ZnO varistors", J. Appl. Phys., Vol. 70, No. 11, p. 6883, 1991.

[4] Y.- S. Lee, K.-S. Liao, and T.- Y. Tseng, "Microstructure and crystal phases of praseodymium in zinc oxides varistor ceramics", J. Amer. Ceram. Soc., Vol. 79, No. 9, p. 2379, 1996.

[5] C.-W. Nahm, C.-H. Park, and H.-S.Yoon, "Microstructure and varistor properties of ZnO-Pr_6O_{11}-CoO-Nd_2O_3 based ceramics", J. Mater. Sci. Lett., Vol. 19, No. 4, p. 271, 2000.

[6] C.-W. Nahm, "The electrical properties and d.c. degradation dharacteristics of Dy_2O_3 doped Pr_6O_{11}-based ZnO varistors", J. Euro. Ceram. Soc., Vol. 21, No. 4, p. 545, 2001.

[7] C.-W. Nahm and C.-H. Park, "Effect of Er_2O_3 addition on the microstructure, electrical properties, and stability of Pr_6O_{11}-based ZnO ceramic varistors", J. Mater. Sci., Vol. 36, No. 7, p. 1671, 2001.

[8] C.-W. Nahm, "The nonlinear properties and stability of ZnO-Pr_6O_{11}-CoO-Cr_2O_3-Er_2O_3 ceramic varistors", Mater. Lett., Vol. 47, No. 3, p. 182, 2001.

[9] C.-W. Nahm and J.-S. Ryu, "Influence of sintering temperature on varistor characteristics of ZPCCE-based ceramics", Mater. Lett., Vol. 53, No. 1-2, p. 110, 2002.

[10] C.-W. Nahm and B.-C. Shin, "Effect of sintering temperature on electrical properties and stability of Pr_6O_{11}-based ZnO varistors", J. Mater. Sci: Mater. Electron., Vol. 12, No. 2, p. 111, 2002.

[11] C.-W. Nahm, "Microstructure and electrical properties of Y_2O_3 doped ZnO-Pr_6O_{11}-based varistor", Mater. Lett., Vol. 57, No. 7, p. 1317, 2003.

[12] C.-W. Nahm and B.-C. Shin, "Highly stable electrical properties of ZnO-Pr_6O_{11}-CoO-Cr_2O_3-Y_2O_3-based varistor cearmics", Mater. Lett., Vol. 57, No. 7, p. 1322, 2003.

[13] J. C. Wurst and J. A. Nelson, "Lineal intercept technique for measuring grain size in two-phase polycrystalline ceramics", J. Amer. Ceram. Soc., Vol. 55, No. 97-12, p. 109, 1972.

[14] J. Fan and R. Freer, "Deep level transient spectroscopy of zinc oxide varistors doped with aluminum oxide and/or silver oxide", J. Amer. Cearm. Soc., Vol. 77, No. 10, p. 2663, 1994.

[15] Alles, A. B., Puskas, R. Callahan, G., and Burdick, V. L., "Compositional effect on the liquid-phasse sintering of praseodymium oxides-based ZnO varistors", J. Am. Ceram. Soc., Vol. 76, No. 8, p. 2098, 1993.